

1    **Supplementary Material:**

2    **1. Description of the new unified treatment of aerosol processing by convective clouds**

3        We begin by briefly reviewing the existing CAM5 treatment. The treatments of deep and  
4        shallow convective clouds in CAM5 are described at length in Neale et al. (2010) and references  
5        therein. The deep convection parameterization is based on Zhang and McFarlane (1995), and  
6        considers an ensemble of updraft and downdraft plumes, although only the ensemble updraft and  
7        downdraft properties are used for aerosol processing. The shallow convective parameterization  
8        is based on Park and Bretherton (2009), represented by a single entraining-detaining updraft  
9        plume. From the standpoint of aerosol processing, the deep and shallow convection treatments  
10       are conceptually very similar. Also, both of the existing treatments of aerosol processing by  
11       convective clouds consider wet removal and vertical transport separately and sequentially.

12       The wet removal of aerosols in CAM5 distinguishes between “in-cloud wet removal”  
13       (activation of interstitial aerosol particles to become cloud-borne aerosol, following by  
14       conversion of cloud-condensate and cloud-borne aerosol to precipitation) and “below-cloud wet  
15       removal” (capture of interstitial aerosol particles by precipitation particles via impaction and  
16       Brownian diffusion). Below-cloud wet removal is identical in the existing and new unified  
17       treatments. Note that CAM5 treats cloud-borne aerosols within stratiform clouds explicitly in a  
18       prognostic manner, and they are assumed to not interact with convective clouds. The  
19       “interstitial” aerosol mixing ratios in the CAM5 code ( $\bar{q}_{AI^*}$ ) are defined to be the sum of  
20       interstitial plus convective-cloud-borne aerosols, expressed as grid-cell averaged quantities. The  
21       convective-cloud-borne aerosols are calculated in the wet removal routines in a diagnostic  
22       manner.

23 The in-cloud aerosol wet removal parameterizations for shallow and deep convection utilize  
 24 profiles of cloud fractional area ( $f_{CLDC}$ ), in-cloud cloud-condensate mixing ratio ( $ICWMR$ , in  
 25 kg/kg), and grid-cell mean precipitation production ( $RPROD$ , in kg/kg/s), to calculate a first-  
 26 order rate loss rate (the rate at which cloud-condensate is converted to precipitation within the  
 27 cloud),

$$28 \quad \lambda_{WETC} = RPROD / (f_{CLDC} ICWMR) . \quad (S1)$$

29 In the CAM5 convective-cloud wet removal, the cloud-borne aerosol mixing ratio within the  
 30 convective cloud is assumed equal to the grid-cell mean interstitial aerosol mixing ratio at that  
 31 level multiplied by a prescribed convective-cloud activation fraction,  $f_{ACTC}$ , which varies with  
 32 aerosol mode and species. Over a model time-step  $\Delta t$ , a fraction  $f_{WETC} = \text{MIN}(\Delta t \lambda_{WETC}, 1)$  of  
 33 this cloud-borne aerosol is removed, and the change to the grid-cell mean interstitial aerosol is

$$34 \quad \Delta \bar{q}_{AI^*} = -0.4 f_{CLDC} f_{WETC} f_{ACTC} \bar{q}_{AI^*} \quad (S2)$$

35 where the 0.4 is a wet removal adjustment factor, applied because  $f_{CLDC}$  and  $f_{WETC}$  from the  
 36 convective parameterizations would otherwise produce too much wet removal.

37 The deep convective vertical transport of aerosols and other trace species follows the  
 38 assumption in the original ZM parameterization that the updrafts and downdrafts are described  
 39 by steady-state bulk plume models representing the ensemble of up- and downdrafts in the  
 40 clouds. Aerosol mixing ratios in the updraft ( $q_{A,U}$ ) and downdraft ( $q_{A,D}$ ) ensembles are calculated  
 41 by integrating steady-state mass continuity equations either upwards or downwards:

$$42 \quad \frac{\partial(M_U q_{A,U})}{\partial p} = E_U (1 - f_{WET}) q_{A,E} - D_U q_{A,U} \quad (S3a)$$

43 
$$\frac{\partial(M_D q_{A,D})}{\partial p} = E_D (1 - f_{WET}) q_{A,E} - D_D q_{A,D} \quad (\text{S3b})$$

44 Here the  $U$ ,  $D$ , and  $E$  subscripts denote updraft, downdraft, and environment,  $M$  is vertical mass  
 45 flux of air (Pa/s),  $E$  is the positive portion of  $\partial M / \partial p$  due to entrainment,  $-D$  is the negative  
 46 portion due to detrainment,  $p$  is pressure, and  $f_{WET}$  is the fractional wet removal of aerosols in the  
 47 convective and stratiform clouds areas. The  $(1-f_{WET})$  factor applied to entrainment accounts for  
 48 wet removal of aerosols that is applied prior to the deep convective transport, providing some  
 49 coupling of wet removal and vertical transport. Also,  $q_{A,E}$  is assumed equal to  $\bar{q}_{AI^*}$ . Equations  
 50 S3a and S3b are solved to determine mixing ratios in the convective up- and downdrafts. The  
 51 grid-cell mean interstitial plus convective-cloud-borne aerosol mixing ratios are then updated by  
 52 solving

53 
$$\frac{\partial \bar{q}_{AI^*}}{\partial t} = -\frac{\partial}{\partial p} [M_U q_{A,U} + M_D q_{A,D} + M_E q_{A,E}] \quad (\text{S4})$$

54 where  $M_E = -(M_U + M_D)$  is the compensating vertical mass flux in the environment. The shallow  
 55 convective transport of aerosols is treated similarly, but the  $(1-f_{WET})$  factor is not applied to  
 56 entrainment, there is no downdraft, and the numerical discretization applied to the (S3-4) differs  
 57 somewhat.

58 The main differences between the new unified treatment of aerosol processing by convective  
 59 clouds and the previous CAM5 treatments are that (1) wet removal and vertical transport are  
 60 treated simultaneously, (2) cloud-borne aerosols and aerosol activation are treated explicitly in  
 61 the updraft, and (3) wet removal is applied to aerosols in the updraft. Similar to the previous

62 treatments, we assume that aerosol mixing-ratio profiles in the updraft and downdraft are steady-  
63 state. The mass-continuity equation for the updraft is:

$$64 \quad \frac{\partial(M_U q_{AX,U})}{\partial p} = E_U q_{AX,E} - D_U q_{AX,U} + A_U (\dot{q}_{AX,U})_{ACT} + A_U (\dot{q}_{AX,U})_{WET} \quad (S5)$$

65 where the  $AX$  subscript is either  $AI$  for an interstitial aerosol species or  $ACC$  for a convective-  
66 cloud-borne (activated) aerosol species. (Note that  $q_{AI}$  is interstitial aerosol only, while  $\bar{q}_{AI*}$   
67 includes the convective-cloud-borne aerosol.) The  $(\dot{q}_{AX,U})_{ACT}$  and  $(\dot{q}_{AX,U})_{WET}$  terms are the rates  
68 of change due to activation and in-cloud wet removal in the updraft, respectively. For the  
69 downdraft, we assume that only interstitial aerosol is entrained from the environment and there is  
70 no aerosol activation as the downdraft is never super-saturated. As a result, the downdraft  
71 contains only interstitial aerosol, and there is no in-cloud wet removal. Thus the downdraft  
72 mass-continuity equation is unchanged from (S3b).

73 Aerosol activation in the updraft includes activation at cloud-base and above cloud-base. The  
74 cloud-base activation uses the Abdul-Razzak and Ghan (2000) parameterization to diagnose the  
75 maximum supersaturation in a rising air parcel and the activation fraction ( $f_{ACTC}$ ) for interstitial  
76 aerosol mass and number of each aerosol mode. This requires an updraft vertical velocity,  $w_U$ ,  
77 which can be diagnosed from  $M_U = \rho A_U w_U g$ , where  $\rho$  is air density,  $A_U$  is updraft fractional  
78 area, and  $g$  is the gravitational constant. The shallow convection parameterization assumes that  
79  $A_U = f_{CLDC}/2$ , and this gives reasonable values for  $w_U$ . The deep convection parameterization  
80 provides no information on  $A_U$ , and using  $A_U = f_{CLDC}/2$  gives unreasonably low values for  $w_U$ .  
81 Thus for deep convection we use empirical values for  $w_U$  based on measurements by Zipser and  
82 Lemone (1980) during GATE. The activation tendency needed in (A5) is then

83  $(\dot{q}_{AI,U})_{ACT} = -(\dot{q}_{ACC,U})_{ACT} = -(f_{ACTC} q_{AI,U}) / \Delta t_U$  (S6)

84 where  $\Delta t_U = \Delta z / w_U$  is the time for updraft air to move across a layer .

85 Several cloud modeling studies (Pinsky and Kahn, 2003; Segal et al., 2003; Yin et al., 2005;  
86 Phillips et al., 2007) suggest that supersaturations of a few tenths of a percent or more may be  
87 achieved in convective clouds above cloud-base, due to strong adiabatic cooling (from high  
88 updraft velocities) and relatively low hydrometeor surface area (due to conversion of cloud  
89 droplets to precipitation particles). Ghan et al. (2012) suggest that supersaturation above cloud-  
90 base should be diagnosed based on a balance between adiabatic cooling and water vapor  
91 condensation onto hydrometeors, but this requires knowledge of both the updraft velocity and  
92 hydrometeor size distribution. This information is lacking or very approximate in the current  
93 CAM5.0 convective cloud parameterizations, so currently we simply prescribe an above cloud-  
94 base supersaturation of 0.3%, based on the several cloud-modeling studies cited above. With  
95 this we can calculate the aerosol activation fractions as done in the Abdul-Razzak and Ghan  
96 (2000) parameterization.

97 The in-cloud wet removal tendency for cloud-borne aerosols in the updraft is given by

98  $(\dot{q}_{ACC,U})_{WET} = -\lambda_{WETC,U} q_{ACC,U}$  (S7a)

99 and the wet-removal first-order loss rate is taken to be

100  $\lambda_{WETC,U} = RPROD / (A_U ICWMR)$  (S7b)

101 This gives

102  $A_U(\dot{q}_{ACC,U})_{WET} = -(RPROD/ICWMR)q_{ACC,U}$  (S7c)

103 After aerosol mixing ratios in the updrafts and downdrafts have been calculated, changes to  
 104 the grid-cell mean aerosol mixing ratios are calculated by solving

105 
$$\frac{\partial \bar{q}_{AX}}{\partial t} = -\frac{\partial}{\partial p} [M_U q_{AX,U} + M_D q_{AX,D} + M_E q_{AX,E}] + A_U(\dot{q}_{AX,U})_{ACT} + A_U(\dot{q}_{AX,U})_{WET} + A_E(\dot{q}_{AX,E})_{RES}$$
 (S8)

106 The right-most term involves resuspension in the environment of cloud-borne aerosols detrained  
 107 from the updraft. Currently we assume complete resuspension for the detrained convective-  
 108 cloud-borne aerosols, so there is no transfer of convective- to stratiform-cloud-borne aerosols.

109 **2. Aerosol and Aerosol-Cloud Processes in the CAM5**

110 We use a developmental version of the stand-alone CAM5, which has nearly identical  
 111 physics to the released version CAM5.1. Aerosol evolution in CAM5 is controlled by a  
 112 combination of emission, transport, aerosol microphysics (new particle formation, condensation,  
 113 coagulation, aging, etc.), and dry and wet removal. Aerosol and cloud microphysics and their  
 114 interactions are described and evaluated by Liu et al. (2012). Here we briefly summarize the  
 115 processes in CAM5 that are relevant to aerosol (BC in particular) and evolution.

116 *1) Aerosol Mixing State and Aging*

117 CAM5 employs a modal aerosol module (MAM) to represent aerosols (Liu et al., 2012). The  
 118 aerosol mixing-state and size distribution is represented by multiple log-normally distributed  
 119 modes, with internal mixing assumed for aerosol species [e.g., sulphate, BC, primary organic  
 120 matter (POM), secondary organic aerosol (SOA)] within each individual mode. Two versions of  
 121 MAM are used in this study: a 3-mode “fast” representation (MAM3) and a more complex 7-

122 mode “benchmark” representation (MAM7). The major difference between MAM3 and MAM7  
123 related to BC lies in the treatment of aging. In MAM3, BC and POM are emitted into the  
124 accumulation mode, which also contains highly-hygroscopic sulphate and sea-salt and  
125 moderately hygroscopic SOA. The freshly emitted BC and POM are thus immediately mixed  
126 with these hygroscopic species in particles that can be viable cloud condensation nuclei (CCN),  
127 depending on the amount of BC/POM emissions versus existing sulphate/sea-salt/SOA. In  
128 MAM7, BC and POM are emitted into a primary carbon mode, which contains no other species.  
129 The hygroscopicity of this mode depends on the assumed POM hygroscopicity which is  
130 generally lower than that of the MAM3 accumulation mode. Thus in MAM7, the freshly emitted  
131 BC and POM are in particles that are less-viable CCN and less likely to experience wet removal.  
132 As hygroscopic species (e.g.,  $H_2SO_4$ ,  $NH_3$  and semi-volatile organic vapors) condense onto  
133 primary carbon mode particles, the particles are “aged” (become more hygroscopic) and are  
134 gradually transferred into the MAM7 accumulation mode. The rate of transfer is controlled by  
135 somewhat uncertain aging parameters, such as the number of mono-layers of sulphate coating  
136 needed to make a fresh BC/POM particle a viable CCN (Liu et al. 2012).

137 *2) Aerosol-Cloud Interactions*

138 In CAM5, aerosol particles are assumed to either be suspended in the air or reside in cloud  
139 droplets, and these are referred to as interstitial and cloud-borne aerosol, respectively. Particles  
140 that are viable CCN and are within the cloudy portion of a grid cell are converted from the  
141 interstitial state to the cloud-borne state through aerosol activation (or nucleation scavenging).  
142 Cloud-borne aerosols in stratiform clouds are treated prognostically in CAM5: their mixing  
143 ratios are saved between model time steps and evolve as a result of source, sink, and transport  
144 processes. Their activation is parameterized using vertical velocity (resolved and sub-grid

145 turbulent) and aerosol properties of all the modes following Abdul-Razzak and Ghan (2000).  
146 Activation may occur when aerosols are carried into clouds from below and when cloud fraction  
147 increases. Therefore, liquid cloud fraction diagnosed from the triangular distribution of grid-  
148 mean relative humidity in CAM5 is critical to aerosol activation. Cloud-borne aerosols in  
149 convective clouds are treated diagnostically: their mixing ratios are diagnosed each model time  
150 step (with no “memory”) from the interstitial aerosol mixing ratios. Cloud-borne BC particles are  
151 returned to the interstitial state upon drop evaporation (i.e., resuspension). The representation of  
152 activation/resuspension processes, and consequent effects on clouds and precipitation in the  
153 model, has direct and indirect impacts on BC wet removal and transport.

154 *3) Removal*

155 Both interstitial and cloud-borne aerosol particles are subject to wet and dry removal  
156 (deposition). CAM5 treats in-cloud and below-cloud wet removal of aerosols. In-cloud wet  
157 removal involves activation of interstitial aerosol to become cloud-borne, followed by  
158 conversion of cloud droplets (and the cloud-borne aerosol particles) to precipitation. The  
159 activation step is described above. The removal rate of cloud-borne aerosol is equal to the rate at  
160 which cloud-water is converted to precipitation, as determined by the model’s cloud  
161 parameterizations. In-cloud wet removal through attachment of interstitial aerosol to ice particles  
162 followed by conversion of ice particles to precipitation is currently not treated. Below-cloud wet  
163 removal involves direct capture of interstitial aerosols by precipitation particles through a  
164 number of processes (e.g., inertial impaction, Brownian diffusion) and is relatively inefficient for  
165 aerosol in the accumulation mode size range. Different tunable parameters, which we refer to as  
166 wet-removal adjustment factors ( $\leq 1$ ), are applied to the calculation of the stratiform/convective  
167 in-cloud and below-cloud scavenging rates to account for various uncertainties from the aerosol

168 mixing state, activation, and model-predicted cloud and precipitation properties (Liu et al.,  
169 2012). When raindrops evaporate below cloud, a portion of the wet-scavenged aerosol is  
170 resuspended as interstitial particles and this produces some downwards redistribution of aerosols.

171 For BC and sulphate (predominately sub-micron) in CAM5, dry removal accounts for about  
172 16-18% and 11-12% of the total removal on a global annual basis (with the ranges reflecting  
173 MAM3 and MAM7 values). Aerosol dry deposition velocities are calculated using the method  
174 developed by Zhang et al. (2001) with model provided aerodynamic resistance, friction velocity,  
175 and surface properties. Gravitational settling is also treated.

176 *4) Transport*

177 Interstitial aerosol particles in CAM5 are transported by resolved winds, turbulence, and  
178 shallow and deep convection. Advection by resolved winds is neglected for cloud-borne aerosols  
179 due to the assumption that aerosol particles in liquid clouds are relatively short-lived (Koch et  
180 al., 2006). Stratiform-cloud-borne aerosols undergo turbulent vertical transport. Ghan and Easter  
181 (2006) showed that neglecting transport of stratiform-cloud-borne aerosols by resolved winds  
182 introduces small global mean biases in aerosol number concentrations at a coarse resolution  
183 ( $2^\circ \times 2.5^\circ$ ). Ma et al. (2012) have compared CAM5 simulations allowed to evolve freely with  
184 simulations constrained by various reanalysis products and found that CAM5 Arctic circulation  
185 patterns (mean and transient eddy) are quite reasonable. This suggests that transport of aerosols  
186 by resolved winds in CAM5 is not a major contributor to the poor simulation of remote Arctic  
187 aerosols.

188 **3. Sensitivity test on Emissions**

189 The simulations discussed in the main text use the IPCC AR5 emissions for year 2000. The  
190 AR5 BC emissions for 1980 are quite different from the 2000 emissions due to a number of

191 socio-economic changes. Although the global annual emissions are lower for 1980 ( $6.9 \text{ Tg C yr}^{-1}$ )  
192 than for 2000 ( $7.8 \text{ Tg C yr}^{-1}$ ), more importantly for the Arctic, as shown in Fig. S1, the DJF  
193 emissions integrated between  $40^{\circ}\text{N}$  and  $70^{\circ}\text{N}$  were significantly higher in 1980 than in 2000  
194 ( $1.87 \text{ vs. } 1.25 \text{ Tg C yr}^{-1}$ ). At these latitudes, the summer (JJA) BC emissions are higher than  
195 winter due to wildfire emissions. This summer increase is lower in 1980 than in 2000 (the ratios  
196 of JJA to DJF emissions for  $40\text{-}70^{\circ}\text{N}$  are 1.12 and 1.46 respectively), and this could make a  
197 difference to the seasonal cycle of Arctic BC. It should be noted that the AR5  $\text{SO}_2$  emissions for  
198 years 1980 and 2000 have the similar difference in DJF between  $40^{\circ}\text{N}$  and  $70^{\circ}\text{N}$  (113% higher  
199 emission in 1980; figure not shown).

200 Figure S2 compares simulated DJF BC in two identical simulations (based on the ALL\_m7  
201 configuration) but with the 1980 emissions and 2000 emissions, respectively. The zonal-mean  
202 BC burden is smaller in the 1980 simulation south of  $40^{\circ}\text{N}$  (consistent with the distribution of  
203 BC emissions) but is larger (by a factor of 1.5) from  $50^{\circ}\text{N}$  to  $90^{\circ}\text{N}$ . Previous studies have  
204 identified N. Europe and Russia as major source regions for Arctic haze (Shindell et al., 2008;  
205 Matsui et al., 2011), and the large 1980 to 2000 emissions change between  $40^{\circ}\text{N}$  and  $70^{\circ}\text{N}$  is  
206 likely responsible for the difference in Arctic BC between the two simulations. Larger total  
207 burden leads to larger cloud-borne burden and wet deposition flux as well, but the total removal  
208 rates are almost identical in the two simulations (see Fig. S2b). The Arctic sulphate burden and  
209 surface mixing ratios are doubled under the 1980 emissions scenario due to the even larger  
210 increase in  $\text{SO}_2$  emission than in 2000 (figure not shown).

211 With the 1980 emission, the predicted surface BC and sulphate seasonality over the Arctic  
212 sites is further improved. This is because of the stronger DJF sources between  $40^{\circ}\text{-}70^{\circ}\text{N}$  in the

213 1980 emission inventory than in the 2000's, which more effectively increases the Arctic BC and  
214 sulphate mixing ratios (from the surface to about 600 hPa) than sources from lower latitudes.

215 **4. Tables for model-observation comparison**

216 Table S1 summarizes how the modifications to CAM5 impact the simulated surface-level  
217 BC compared to observations from three networks/compilations. In Liu et al. (2011b) and Wang  
218 et al. (2011a), simulated BC are compared to observations from the IMPROVE and EMEP  
219 networks and the combined compilations of Liousse et al. (1996) and Cooke et al. (1999). Table  
220 S1 lists the multi-site means and medians for these three datasets and additionally for the Zhang  
221 et al. (2008) China dataset. The changes between the various simulations are considerably  
222 smaller at these surface sites than the changes to the global annual burdens (Table 2 in the text).  
223 This is not surprising for the IMPROVE and EMEP networks, where the sites are in the  
224 continental US and Europe, relatively close to sources. The slower BC aging has small impacts  
225 for the same reasons. The unified convection treatment lowers the simulated values at the sites  
226 slightly, although it increases the global burden. The simulation with 1980 emissions has  
227 noticeably higher mixing ratios over the IMPROVE and EMEP network sites because of  
228 emissions changes in these regions. The simulated values for the base model configurations are  
229 lower than observed, so model changes that increase BC burden and transport to the Arctic also  
230 reduce the CAM5 low-bias for these datasets. All the simulations strongly underestimate the  
231 China observations from Zhang et al. (2008), suggesting that BC emissions for this region may  
232 be significantly underestimated. One of the most notable features is that the MMF simulation  
233 gives much lower surface mixing ratios for the three datasets than the CAM5std and the CTRL  
234 simulation, although the MMF global burden is about 50% higher. As shown in the BC vertical  
235 distributions (see Figs. 9, 10 and 11), CAM5 often predicts a stronger near-surface peak than the

236 MMF at low- and mid-latitudes, suggesting stronger boundary-layer turbulent mixing and  
237 vertical transport in the MMF. Correlation coefficients (not shown) vary only slightly between  
238 the simulations, one exception being the 1980 emissions simulation and EMEP Network, but the  
239 correlations are all rather low for that dataset.

240 Table S2 provides similar information for surface-level sulphate, using observations from the  
241 IMPROVE, EMEP, and U. Miami (marine sites) networks. The changes between the various  
242 simulations are larger than those for BC, but the changes are still smaller than the global annual  
243 burden changes. As with BC, the changes increase sulphate mixing ratios, which increase the  
244 high bias for the IMPROVE and EMEP continental sites, but improve (and even reverse) the low  
245 bias for the U. Miami remote marine sites. The new unified convection (CONV) increases  
246 surface mixing ratios, compared to the slight decrease for BC, which we attribute to their  
247 different sources (locations and primary vs. secondary). Correlation coefficients again vary only  
248 slightly between the simulations, except for the 1980 emissions simulation and EMEP Network.

### References (for Supplementary Material):

Abdul-Razzak, H., and S. J. Ghan (2000), A parameterization of aerosol activation 2. Multiple aerosol types, *J. Geophys. Res.-Atmos.*, 105(D5), 6837–6844.

Bond, T. C., Bhardwaj, E., Dong, R., Jogani, R., Jung, S. K., Roden, C., Streets, D. G., and Trautmann, N. M.: Historical emissions of black and organic carbon aerosol from energy-related combustion, 1850–2000, *Global Biogeochem. Cy.*, 21(2), Gb2018, doi:10.1029/2006gb002840, 2007.

Cooke, W. F., C. Liousse, H. Cachier, and J. Feichter (1999), Construction of a 1 degrees×1 degrees fossil fuel emission data set for carbonaceous aerosol and implementation and radiative impact in the ECHAM4 model, *J. Geophys. Res.*, 104, 22137–22162.

Ghan, S. J. and Easter, R. C.: Impact of cloud-borne aerosol representation on aerosol direct and indirect effects, *Atmos. Chem. Phys.*, 6, 4163–4174, doi:10.5194/acp-6-4163-2006, 2006.

Koch, D., Schmidt, G. A., and Field, C.: Sulfur, sea salt and radionuclide aerosols in GISS ModelE, *J. Geophys. Res.*, 111, D06206, doi:10.1029/2004JD005550, 2006.

Liousse, C., et al. (1996), A global three-dimensional model study of carbonaceous aerosols, *J. Geophys. Res.*, 101, 19411–19432.

Neale, R. B., Chen, C.-C., Gettelman, A., Lauritzen, P. H., Park, S., Williamson, D. L., Conley, A. J., Garcia, R., Kinnison, D., Lamarque, J.-F., Marsh, D., Mills, M., Smith, A. K., Tilmes, S., Vitt, F., Cameron-Smith, P., Collins, W. D., Iacono, M. J., Easter, R. C., Ghan, S. J., Liu, X., Rasch, P. J., and Taylor, M. A.: Description of the NCAR Community Atmosphere Model (CAM 5.0), NCAR/TN-???+STR, 2010.

Park, S., and C. S. Bretherton (2009), The University of Washington shallow convection and moist turbulence schemes and their impact on climate simulations with the Community Atmosphere Model, *J. Climate*, 22(12), 3449–3469, doi:10.1175/2008jcli2557.1.

Phillips, V. T. J., L. J. Donner, and S. T. Garner (2007), Nucleation processes in deep convection simulated by a cloud-system-resolving model with double-moment bulk microphysics, *J Atmos Sci*, 64(3), 738-761.

Pinsky, M. B., and A. P. Khain (2002), Effects of in-cloud nucleation and turbulence on droplet spectrum formation in cumulus clouds, *Q J Roy Meteor Soc*, 128(580), 501-533.

Segal, Y., M. Pinsky, A. Khain, and C. Erlick (2003), Thermodynamic factors influencing bimodal spectrum formation in cumulus clouds, *Atmos Res*, 66(1-2), 43-64.

Yin, Y., K. S. Carslaw, and G. Feingold (2005), Vertical transport and processing of aerosols in a mixed-phase convective cloud and the feedback on cloud development, *Q J Roy Meteor Soc*, 131(605), 221-245.

Yttri, K. E., et al. (2007), Elemental and organic carbon in PM<sub>10</sub>: a one year measurement campaign within the European Monitoring and Evaluation Programme EMEP, *Atmos. Chem. Phys.*, 7, 5711-5725, doi:10.5194/acp-7-5711-2007.

Zhang, G. J., and N. A. McFarlane (1995), Sensitivity of climate simulations to the parameterization of cumulus convection in the Canadian Climate Center general-circulation model, *Atmos. Ocean*, 33(3), 407–446.

Zhang, L. M., Gong, S. L., Padro, J., and Barrie, L.: A size-segregated particle dry deposition scheme for an atmospheric aerosol module, *Atmos. Environ.*, 35(3), 549–560, 2001.

Zhang, X. Y., et al. (2008), Carbonaceous aerosol composition over various regions of China during 2006, *J. Geophys. Res.*, 113, D14111, doi: 10.1029/2007JD009525.

Zipser, E. J., and M. A. Lemone (1980), Cumulonimbus Vertical Velocity Events in Gate. Part II: Synthesis and Model Core Structure, *J Atmos Sci*, 37, 2458-2469.

Table S1: Observed and simulated multi-site mean and median BC (in  $\text{ng m}^{-3}$ , with medians in parentheses) for IMPROVE network sites (annual means), EMEP network sites (annual means), Zhang et al. (2008) China sites, and Liousse et al. (1996) and Cooke et al. (1999) compilations (various time periods; L96&C99). The IMPROVE, EMEP, and Liousse-Cooke sites correspond to Figures 11a, 11b, and 13b of Liu et al. (2011b), respectively.

<b>Case</b>	<b>IMPROVE</b>	<b>EMEP*</b>	<b>China**</b>	<b>L96&amp;C99</b>
<b>Observed</b>	257. (215.)	730. (620.)	3015. (3600.)	398. (123.)
<b>MMF</b>	148. (119.)	295. (290.)	652. ( 614.)	179. ( 47.)
<b>CAM5std</b>	206. (153.)	410. (391.)	891. ( 854.)	242. ( 61.)
<b>CTRL</b>	214. (158.)	423. (413.)	948. ( 914.)	256. ( 51.)
<b>CONV</b>	214. (160.)	409. (397.)	906. ( 882.)	242. ( 57.)
<b>CONV_sact</b>	209. (156.)	396. (387.)	918. ( 885.)	239. ( 65.)
<b>CONV_FD</b>	215. (166.)	422. (400.)	950. ( 905.)	247. ( 74.)
<b>CONV_SF</b>	218. (166.)	435. (416.)	968. ( 901.)	257. ( 67.)
<b>CONV_m7</b>	226. (170.)	430. (409.)	990. ( 914.)	260. ( 66.)
<b>ALL_m3</b>	222. (172.)	436. (412.)	967. ( 904.)	252. ( 64.)
<b>ALL_m7</b>	238. (190.)	476. (424.)	1049. ( 995.)	277. ( 75.)

\* The 2 “urban background” sites (see Table 1 of Yttri et al., 2007) are excluded.

\*\* The 5 sites in the “urban group” (see Table 2 of Zhang et al., 2008) are excluded.

Table S2: Observed and simulated multi-site means and medians for annual average sulphate (in  $\mu\text{g m}^{-3}$ , with medians in parentheses) for IMPROVE, EMEP, and University of Miami network sites. The IMPROVE, EMEP, and U. Miami sites correspond to Figures 9a, 9b, and 10 of Liu et al. (2011b), respectively.

Case	IMPROVE	EMEP	U. Miami
<b>Observed</b>	1.59 (0.98)	2.37 (2.18)	0.94 (0.43)
<b>MMF</b>	2.17 (1.81)	2.64 (2.80)	1.01 (0.61)
<b>CAM5std</b>	2.06 (1.63)	2.27 (2.39)	0.63 (0.35)
<b>CTRL</b>	2.23 (1.74)	2.44 (2.50)	0.68 (0.35)
<b>CONV</b>	2.37 (1.90)	2.52 (2.59)	0.83 (0.49)
<b>CONV_sact</b>	2.30 (1.85)	2.39 (2.48)	0.81 (0.42)
<b>CONV_FD</b>	2.44 (1.92)	2.62 (2.67)	0.87 (0.50)
<b>CONV_SF</b>	2.59 (2.05)	2.79 (2.94)	0.93 (0.54)
<b>CONV_m7</b>	2.44 (1.87)	3.10 (3.31)	0.87 (0.52)
<b>ALL_m3</b>	2.60 (2.00)	2.84 (2.92)	0.89 (0.54)
<b>ALL_m7</b>	2.74 (2.04)	3.64 (3.92)	0.97 (0.59)

Table S3: Observed (as listed in Table 1 of Wang et al., 2011b) and simulated global annual mean LWP, total precipitation rate (PRECT), residual fluxes at surface (RESSURF) and top of the model atmosphere (RESTOM) and cloud forcing (SWCF and LWCF).

Case	LWP ( $\text{g m}^{-2}$ )	IWP ( $\text{g m}^{-2}$ )	PRECT ( $\text{mm d}^{-1}$ )	SWCF (W $\text{m}^{-2}$ )	LWCF ( $\text{W m}^{-2}$ )
<b>Observed</b>	(50,87)	-	2.61	(-46, -53)	(27, 31)
<b>MMF</b>	55.88	9.87	2.85	-50.48	25.96
<b>CAM5std</b>	41.15	17.77	2.96	-49.12	23.67
<b>CTRL</b>	41.04	17.17	2.98	-48.19	22.78
<b>CONV</b>	47.02	17.30	2.95	-51.42	23.78
<b>CONV_sact</b>	46.22	17.79	2.94	-52.06	24.74
<b>CONV_FD</b>	47.30	17.19	2.93	-50.17	23.60
<b>CONV_SF</b>	48.82	17.46	2.94	-52.00	24.03
<b>CONV_m7</b>	46.84	16.94	2.93	-50.64	23.40
<b>ALL_m3</b>	48.62	17.76	2.92	-51.60	24.84
<b>ALL_m7</b>	48.13	17.46	2.90	-50.69	24.39

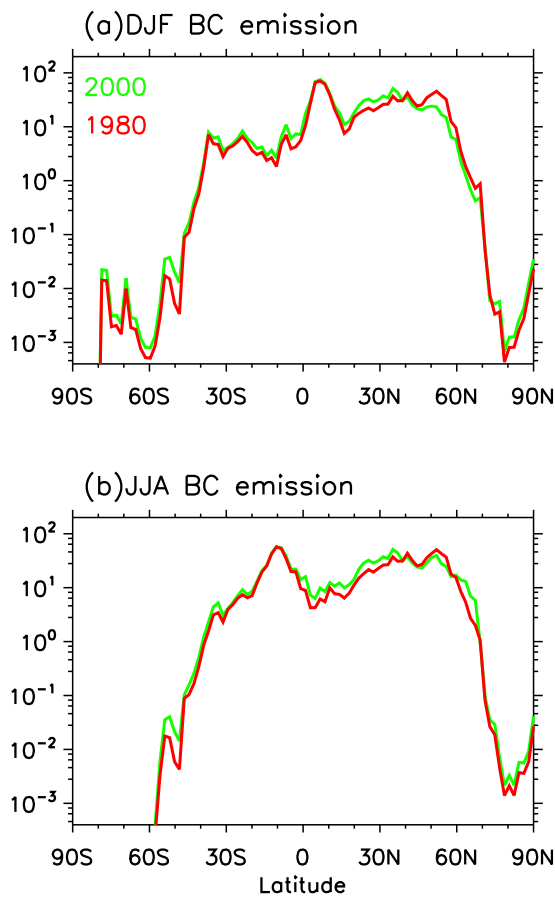


Figure S1: Seasonal zonal-mean BC emission rates ( $kg\ C\ km^{-2}\ yr^{-1}$ ) for the year of 2000 and 1980 in (a) DJF and (b) JJA months.

BC DJF NEW\_m7\_80e/NEW\_m7

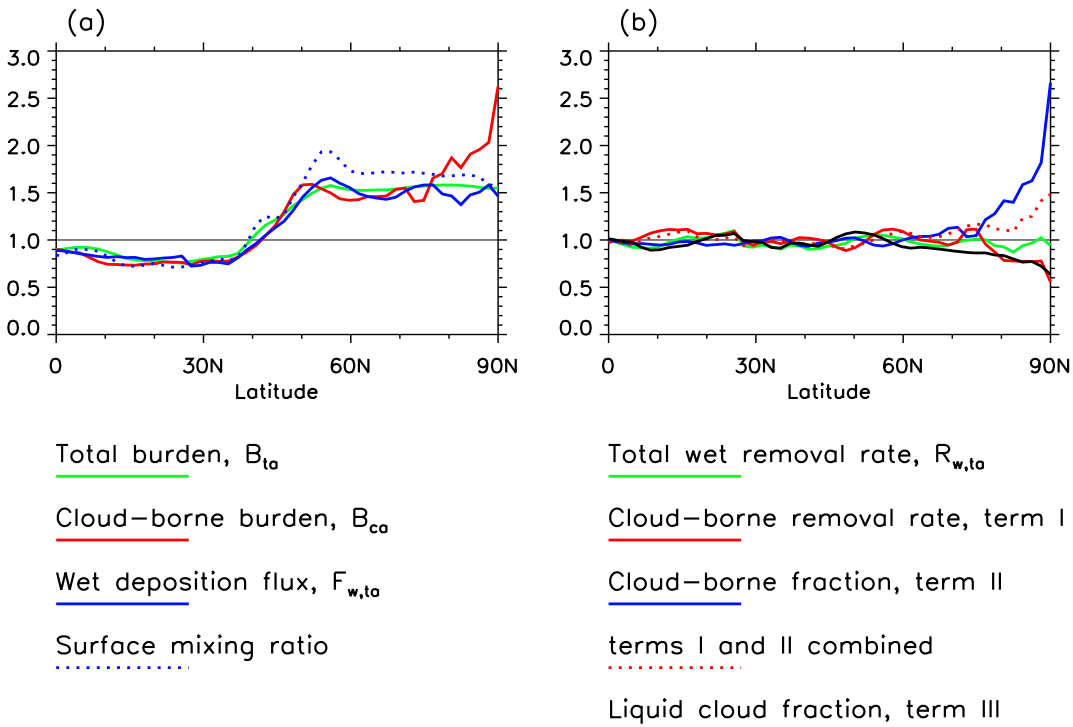


Figure S2: the ratios of the quantities related to BC burden and wet removal, as described in Eqs. (1-3) in the text, derived from two CAM5 simulations (close to the ALL\_m7 setup) with year 1980 emissions and 2000 emissions respectively. Quantities are averaged zonally and over the Northern Hemisphere winter months (DJF).